Treatment of Prostate Cancer with CD46-targeted ^{225}Ac Alpha Particle Radioimmunotherapy

Anil P. Bidkar[1], Sinan Wang[1], Kondapa Naidu Bobba[1], Emily Chan[2], Scott Bidlingmaier[3], Emily A. Egusa[4,5], Robin Peter[1,6], Umama Ali[1], Niranjan Meher[1], Anju Wadhwa[1], Suchi Dhrona[1], Chandrashekhar Dasari[7], Denis Beckford-Vera[1], Yang Su[3], Ryan Tang[1], Li Zhang[8], Jiang He[9], David M. Wilson[1,5], Rahul Aggarwal[4,5], Henry F. VanBrocklin[1], Youngho Seo[1,5], Jonathan Chou[4,5], Bin Liu[3,5], and Robert R. Flavell[1,5,10]

ABSTRACT

Purpose: Radiopharmaceutical therapy is changing the standard of care in prostate cancer and other malignancies. We previously reported high CD46 expression in prostate cancer and developed an antibody–drug conjugate and immunoPET agent based on the YS5 antibody, which targets a tumor-selective CD46 epitope. Here, we present the preparation, preclinical efficacy, and toxicity evaluation of [^{225}Ac]DOTA-YS5, a radioimmunotherapy agent based on the YS5 antibody.

Experimental Design: [^{225}Ac]DOTA-YS5 was developed, and its therapeutic efficiency was tested on cell-derived (22Rv1, DU145), and patient-derived (LTL-545, LTL484) prostate cancer xenograft models. Biodistribution studies were carried out on 22Rv1 tumor xenograft models to confirm the targeting efficacy. Toxicity analysis of the [^{225}Ac]DOTA-YS5 was carried out on nu/nu mice to study short-term (acute) and long-term (chronic) toxicity.

Results: Biodistribution study shows that [^{225}Ac]DOTA-YS5 agent delivers high levels of radiation to the tumor tissue (11.64% ± 1.37%ID/g, 28.58% ± 10.88%ID/g, 29.35% ± 7.76%ID/g, and 31.78% ± 5.89%ID/g at 24, 96, 168, and 408 hours, respectively), compared with the healthy organs. [^{225}Ac]DOTA-YS5 suppressed tumor size and prolonged survival in cell line–derived and patient-derived xenograft models. Toxicity analysis revealed that the 0.5 μCi activity levels showed toxicity to the kidneys, likely due to redistribution of daughter isotope ^{213}Bi.

Conclusions: [^{225}Ac]DOTA-YS5 suppressed the growth of cell-derived and patient-derived xenografts, including prostate-specific membrane antigen–positive and prostate-specific membrane antigen–deficient models. Overall, this preclinical study confirms that [^{225}Ac]DOTA-YS5 is a highly effective treatment and suggests feasibility for clinical translation of CD46-targeted radioligand therapy in prostate cancer.

Introduction

Prostate cancer is the most diagnosed noncutaneous malignancy and second leading cause of death in men worldwide in the year 2021 (1). While early-stage tumors may be effectively treated with surgery, radiation, or androgen deprivation therapy, a significant fraction of patients progress to metastatic, castration-resistant prostate cancer (mCRPC), which is refractory to these treatments. Therapeutic options for patients with mCRPC include androgen signaling inhibitors, chemotherapy, immunotherapy, and radiopharmaceutical therapies including ^{177}Lu-PSMA-617 (Lu-177 vipivotide tetraxetan) or ^{223}Ra (2, 3). Those treatments are not curative, and patients eventually progress. As such, there is a need for preclinical and translational development of new treatments.

In prostate cancer, prostate-specific membrane antigen (PSMA)-targeted radiopharmaceutical therapies have overwhelmingly attracted the most attention. PSMA is a type II glycoprotein overexpressed on prostate cancer cells. Currently, PSMA PET imaging using ^{68}Ga-PSMA-11 or ^{18}F-DCFPyL is used in routine clinical care to localize and stage patients, and ^{177}Lu-PSMA-617 may be used for treatment (4). However, a significant fraction of patients with mCRPC are PSMA negative at diagnosis or develop PSMA negativity on imaging over the course of treatment (5–8). Intrapatient heterogeneity of PSMA expression is one of the reasons for resistance to the PSMA-directed therapies (9). In addition, the prolonged treatment with androgen deprivation therapy could also result in treatment-emergent neuroendocrine/small cell prostate cancer (t-SCNC) with low PSMA expression (10). Therefore, there is a need to identify and evaluate other targets in mCRPC.

We have previously used a non–gene expression–based approach to identify novel tumor cell surface targets, including conformational and posttranslationally modified epitopes. We selected, by laser capture microdissection, billion-member phage human antibody display libraries on prostate cancer patient specimens following counter selection on normal cells and tissues, and identified a panel of human antibodies binding to tumor selectively *in vitro* and *in vivo* (11–13). We

[1]Department of Radiology and Biomedical Imaging, University of California, San Francisco, California. [2]Department of Pathology, University of California, San Francisco, California. [3]Department of Anesthesia, University of California, San Francisco, San Francisco, California. [4]Division of Hematology/Oncology, Department of Medicine, University of California, San Francisco, California. [5]UCSF Helen Diller Family Comprehensive Cancer Center, San Francisco, California. [6]Department of Nuclear Engineering, University of California, Berkeley, California. [7]Department of Surgery, Cardiovascular Research Institute, University of California San Francisco, San Francisco, California. [8]Department of Medicine and the Department of Epidemiology and Biostatistics, University of California, Berkeley, California. [9]Department of Radiology and Medical Imaging, University of Virginia, Charlottesville, Virginia. [10]Department of Pharmaceutical Chemistry, University of California, San Francisco, California.

A.P. Bidkar and S. Wang contributed equally to this article.

Corresponding Authors: Robert R. Flavell, University of California, San Francisco, 185 Berry Street, San Francisco, CA 94143. Phone: 415-353-3638; E-mail: robert.flavell@ucsf.edu; and Bin Liu, bin.liu@ucsf.edu

Clin Cancer Res 2023;XX:XX–XX

doi: 10.1158/1078-0432.CCR-22-3291

Translational Relevance

Radiopharmaceutical therapies are changing the standard of care in prostate cancer, led by agents targeting prostate-specific membrane antigen (PSMA). However, many patients have either primary or acquired resistance to this treatment, often due to loss of target expression. Earlier we reported that CD46 is overexpressed on PSMA-negative or PSMA-positive patients, and this overexpressed CD46 can be targeted for imaging using immunoPET. Herein, we develop the alpha particle radioimmunotherapy agent [^{225}Ac]DOTA-YS5, which shows tumor targeting and antitumor potential in preclinical models including PSMA-negative cell line–derived and patient-derived xenografts. [^{225}Ac]DOTA-YS5 holds great potential to become alpha particle therapy agent for use in patients with metastatic prostate cancer.

identified one of the target antigens as CD46 (14). CD46 is best known for being a negative regulator of the complement activation process (15). We showed that CD46 maintains a high level of expression in prostate cancer across differentiation patterns (14). Compared with PSMA, CD46 is more homogeneously expressed, especially in patients who become resistant to androgen blockade, including t-SCNC (14). As YS5 binds to cancer specific epitope, little binding is observed in healthy tissues, with the exception of placental trophoblasts, and to a lesser extent the prostate epithelium (14). We developed and optimized a CD46-targeting human antibody, YS5, which binds to a tumor-selective conformational epitope, enabling therapeutic targeting of CD46. We have developed an antibody–drug conjugate (ADC) based on YS5, demonstrated its preclinical efficacy in xenograft models, and shown that it is well tolerated in non-human primates (14). The ADC (FOR46) is being tested in patients with mCRPC, as a single agent (phase I, NCT03575819) and a combination treatment (phase I/II, NCT05011188), with promising early results reported previously (16). To enable patient stratification, we have also developed an immunoPET agent based on YS5, ([^{89}Zr]DFO-YS5), and shown that it detects adenocarcinoma, neuroendocrine prostate cancer (NEPC), and PSMA-positive or -negative tumor xenografts in preclinical studies (17). A first-in-human study of this PET agent is ongoing in patients with mCRPC (NCT05245006).

Radioimmunotherapy (RIT) exploits target-specific affinity agents to deliver therapeutic radioisotopes specifically to the target tissue. By using an antibody-based targeting approach, many RIT agents have been produced for clinical applications. Alpha-particle therapies demonstrate both potential advantages as well as limitations when compared with other radiopharmaceutical therapy methods, including greater efficacy, but also at the cost of potentially increased toxicity. Actinium-225 (^{225}Ac), an alpha-emitting radionuclide, is being explored for prostate cancer and other malignancies (18). The advantage of using ^{225}Ac is that it has a long half-life of 9.9 days, and it decays by emitting net four alpha particles generated from ^{221}Fr (6.3 MeV), ^{217}At (7.1 MeV), ^{213}Bi (5.8 MeV), and ^{213}Po (8.4 MeV). Early clinical studies in mCRPC show that ^{225}Ac-PSMA-617 has efficacy, although treatment is associated with xerostomia, and the daughter isotopes are believed to accumulate in kidneys, causing renal toxicity (19). A number of investigators are evaluating ^{225}Ac-labeled small molecules or antibodies for prostate cancer in both preclinical and clinical studies (20, 21). These studies reveal potential for ^{225}Ac-based radiopharmaceutical therapy in prostate cancer, although none of the agents have yet emerged as clinical standard of care. Herein, we report the development and preclinical evaluation of an alpha-particle therapy against CD46 by labeling the anti-CD46 antibody (YS5) with ^{225}Ac ([^{225}Ac]DOTA-YS5).

Materials and Methods

Cell binding assays

[^{225}Ac]DOTA-YS5 binding as well as internalized fractions were determined using 22Rv1 and DU145 cells. The detailed experimental procedure has been given in Supplementary Data.

Animal studies

All the animal experiments were carried out in compliance with Institutional Animal Care and Use Committee established guidelines at Laboratory Animal Resource Center, University of California, San Francisco, CA. All the mice used in our studies were male mice. Methods for animal studies including toxicity, subcutaneous xenograft preparation, patient-derived xenograft (PDX) inoculation, and micro-PET scan (for ^{68}Ga-PSMA11, [^{89}Zr]DFO-YS5 imaging and biodistribution) were described in the Supplementary Data.

Antibody conjugation and ^{225}Ac radiolabeling

The YS5 human IgG1 antibody was produced in HEK293 cells (ATCC, RRID:CVCL_0045) following transient transfection, and produced by protein affinity chromatography followed by ion exchange chromatography as described previously (14). The conjugation of p-SCN-Bn-DOTA on YS5 was carried out according to our previously published method with slight modifications (17). Briefly, YS5 (5 mg) in HEPES buffer was exchanged with 0.1 mol/L Na_2CO_3/$NaHCO_3$ buffer (pH = 9.0) using YM30K centrifugal filter unit (Amicon ultra-0.5 mL, regenerated cellulose, Merck Millipore Ltd.). It was further diluted with 0.1 mol/L Na_2CO_3/$NaHCO_3$ buffer (pH = 9.0) to adjust the final volume to 1 mL. A total of 20 eq. of p-SCN-Bn-DOTA in DMSO (4.5 mg, 20 μL) was added to the solution containing 5 mg of YS5 followed by incubation at 37°C for 1 hour. The reaction mixture was purified using a PD10 gel filtration column by eluting with 0.25 mol/L NaOAc buffer, pH = 6. The DOTA-conjugated YS5 was stored in −20°C until the radiolabeling reactions.

For radiolabeling, 1 mCi of ^{225}Ac$(NO_3)_3$ was received from Oak Ridge National Laboratory by the ^{229}Th decay pathway in solid form, and it was dissolved in 0.2 mol/L HCl (100 μL). The radiolabeling was performed by incubating the 50 μCi (6 μL) of ^{225}Ac$(NO_3)_3$, 2 mol/L NH_4OAc (50 μL, pH = 5.8), L-Ascorbic acid (20 μL, 150 mg/mL), and YS5-DOTA (200 μg, 15.64 μL, 12.785 mg/mL) at 40°C for 2 hours. The radiolabeling progress was monitored by radio thin layer chromatography (TLC) by eluting with a mobile phase 10 mmol/L EDTA (pH = 5.5) on iTLC-SG (Gelman Science Inc.). The radiolabeled antibody was diluted with 300 μL of 0.9% saline, transferred to a YM30K centrifugal filtration unit (Millipore), and centrifuged at 10,640 × *g* for 10 minutes. Then, 200 μL of 0.9% saline was added to the centrifugal filtration unit, followed by centrifugation at 10,640 × *g* for 5 minutes. The [^{225}Ac]DOTA-YS5 (20 μCi, 40%) conjugate was isolated, and the purity was assessed by radio-TLC [iTLC-SG 10 mmol/L EDTA (pH = 5)] immediately after purification.

[^{225}Ac]DOTA-YS5 stability studies

To confirm the stability and aggregation of the radiolabeled antibody, size exclusion chromatography (SEC) was performed. For this, a Merck Hitachi LaChrom Elite system comprised of an L-2130 Pump, L-2200 autosampler, L-2450 DAD detector, L-2400 UV detector, and Carrol and Ramsey Associates model 105S radioactivity detector was

utilized. 1X PBS buffer was used as a mobile phase using a column BioSep 5 μmol/L SEC-s3000 290 Å (Phenomenex, Inc.) with a flow rate of 1 mL per minute. One-mL fractions were collected and then counted on Hidex automatic gamma counter when secular equilibrium was reached at 24 hours. The chromatogram was plotted as counts per minute (CPM) versus time. The stability of the purified radioimmunoconjugate [^{225}Ac]DOTA-YS5 (0.05 mL, 7.43 μCi) was verified by incubating with human serum (0.45 mL; Sigma-Aldrich) and 0.9% saline (0.45 mL, Medline) at 37°C at various timepoints (0 hour, 1 day, 2 days, 3 days, 4 days, 5 days, 7 days, and 14 days). At each timepoint, an aliquot of 8 μL was spotted in duplicate on iTLC-SG and eluted with 10 mmol/L EDTA (pH = 5.5). The decomplexation was monitored by radio TLC and allowed for 24 hours to reach secular equilibrium before counting on a BioScan Ar 2000 radio-TLC Imaging scanner.

[^{225}Ac]DOTA-YS5 biodistribution

To study the biodistribution of [^{225}Ac]DOTA-YS5, 22Rv1 xenograft-bearing mice were used. These mice with tumor volumes ranging from 200 to 300 mm^3 received a 0.5 μCi activity of [^{225}Ac]DOTA-YS5 (specific activity 0.1 μCi/μg) via tail vein injections. Following this, the blood, tumor, and selected organs were collected after 24 hours (day 1), 48 hours (day 2), 96 hours (day 4), 168 hours (day 7), 264 hours (day 11), 336 hours (day 14), and 408 hours (day 17) to study activity present in the tissue. Following this, the presence of [^{225}Ac]DOTA-YS5 in each organ was counted (gamma energy window: 25 to 2,000 keV) with the gamma counter (HIDEX). The standards of injected dose activity were measured in a similar fashion to calculate the %ID/g for each organ without reaching secular equilibrium.

Histology and immunofluorescence staining

Methodology for histology and immunofluorescence staining of the mice organs as well as tumor tissue has been included in the Supplementary Data.

Ionizing radiation quantum imaging detector camera alpha-particle imaging

To study the distribution of [^{225}Ac]DOTA-YS5 within the tissue, iQID (ionizing radiation quantum imaging detector) camera imaging was performed. For this, tumor, liver, kidneys, spleen, heart, and lung tissues from the mice injected with a 0.5 μCi activity of [^{225}Ac]DOTA-YS5 were collected in an Optimum Cutting Temperature (OCT) medium. The tissues in OCT were sliced (20-μm thick) and mounted with a scintillator on the iQID camera (QScint Imaging Solutions, LLC) and acquisition of alpha particles was done for 24 hours at 1.5 V.

Treatment studies with [^{225}Ac]DOTA-YS5

For all treatment studies, the body weights and tumor measurements for each mouse were measured until the mice reached a humane endpoint including body condition score below 2, weight loss by 20%, or tumor volume of 2,000 mm^3. The tumor measurements were carried out twice a week, and tumor volumes were calculated by formula $V = [\text{length} \times (\text{width})^2]/2$.

Animals were randomized in groups, and [^{225}Ac]DOTA-YS5 injections were performed when the tumor reached 100 mm^3. The 22Rv1 and DU145 xenograft-bearing mice were injected with saline, 0.25 μCi, or 0.5 μCi of [^{225}Ac]DOTA-YS5 (specific activity 0.1 μCi/μg). In addition, a separate group received a 0.5 μCi dose of [^{225}Ac]DOTA-IgG. For fractionated dose study, the treatment group was administered with three doses of 0.125 μCi of [^{225}Ac]DOTA-YS5 on day 1, day 37, and day 49.

The LTL-545–bearing mice were injected with saline and [^{225}Ac]DOTA-YS5 (0.03, 0.06, 0.12, and 0.25 μCi) with specific activity of 0.11 μCi/μg. For Fc blocking, native IgG (0.5 mg/mouse) was used. Similarly, the LTL-484 mice were injected intravenously with 0.06, 0.12, and 0.25 μCi doses of [^{225}Ac]DOTA-YS5 activity when tumors reached to 100 mm^3.

Statistical analysis

The results reported are presented as mean ± SD and plotted using Graphpad Prism software. To compare the blood cells and liver and kidney function tests between saline control and treated groups, one-way ANOVA was used with Dunnett multiple comparisons test. The significance of median survival from saline control and treatment groups was determined by log-rank (Mantel–Cox) test. Students *t* test was used to compare the number of phospho-γ-H2AX foci in sections from saline-treated and [^{225}Ac]DOTA-YS5–treated mice groups.

Data availability

The data presented in the current study are available within the article and Supplementary Data or from the corresponding author on reasonable request.

Results

CD46 is expressed in PSMA-positive and PSMA-negative prostate cancer PDXs

Western blot analysis of the series of PDXs was carried out to study the expression of CD46 and PSMA. For this study, we utilized well-characterized PDXs from the Living Tumor Laboratory (22–24). As shown in **Fig. 1A**, PSMA expression was restricted to the adenocarcinoma subtypes we evaluated, while CD46 expression was found in not only adenocarcinoma subtypes but also some neuroendocrine prostate cancer models. IHC staining on PDX tissues for PSMA (Supplementary Fig. S1) showed a similar expression pattern to that observed in Western blots. Our previous study reported that PSMA-positive, androgen receptor (AR)-positive (LTL-484, LTL-331) and PSMA-negative, AR-negative (LTL-545, LTL-331R) xenografts could be readily detected with a CD46 PET scan using [^{89}Zr]DFO-YS5 probe, including the LTL-331, LTL-331R, and LTL-545 models (17). LTL-545 and LTL-331R tumor models used in our experiments are neuroendocrine tumors, while LTL-484 and LTL-331 are adenocarcinoma tumors. Herein, we further demonstrate high uptake in the LTL-484 model, calculated at 23.7% ± 4.7%ID/g based on region of interest analysis of microPET/CT images (**Fig. 1B**). Taken together with our prior report, these data demonstrate that CD46 is highly expressed across a panel of clinically relevant PDX, and a high amount of [^{89}Zr]DFO-YS5 can be delivered and detected using PET imaging.

To compare the results of CD46 targeting [^{89}Zr]DFO-YS5 with a clinically used PSMA targeting probe, we performed microPET/CT scans and biodistribution (**Fig. 1C** and **D**; Supplementary Table S1) using ^{68}Ga-PSMA11 in LTL-545, LTL-484, LTL-331, and LTL-331R PDXs. Tumor uptake of ^{68}Ga-PSMA11 was low to moderate; %ID/g for LTL-545, LTL-484, LTL-331, and LTL-331R was found to be 3.32 ± 0.40, 4.41 ± 1.11, 2.29 ± 0.82, and 0.43 ± 0.13, respectively (**Fig. 1D**). The uptake seen in the LTL-545 model, which is unexpected because of low PSMA expression by Western blotting analysis, may be attributable to differences in vascularity, or to non–PSMA-mediated binding as described recently (22). These data suggest that CD46 is an actionable target in prostate cancer for imaging and therapy using the YS5 antibody, including in PSMA-low and -negative tumors.

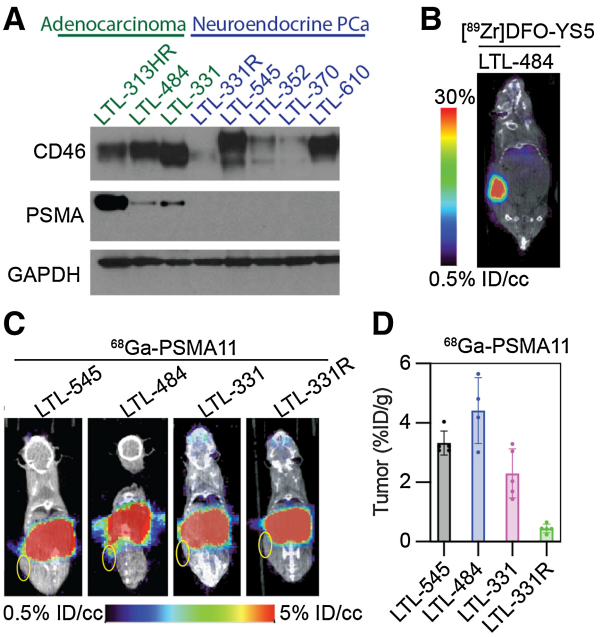

Figure 1.

CD46 is a target for therapy in prostate cancer, including in PSMA-negative disease. **A,** Western blot analysis of the PDX tumors showing overexpression of CD46 in PSMA-positive as well as PSMA-negative tumors. **B,** MicroPET/CT image for detection of the LTL-484 model with the [^{89}Zr]DFO-YS5 probe at 4 days after injections ($n = 4$). **C,** Coronal microPET/CT images for LTL-545, LTL-484, LTL-331, and LTL-331R using ^{68}Ga-PSMA-11. Tumor regions are shown by yellow ellipses ($n = 5$). **D,** Comparison of the tumor uptake of ^{68}Ga-PSMA-11 in PDX model shows low to moderate uptake of ^{68}Ga-PSMA-11 in the indicated PDX models (data represented as mean ± SD, $n = 5$).

Conjugation of DOTA to YS5 and ^{225}Ac radiolabeling

We adopted a standard approach for antibody radiolabeling utilizing DOTA chelator and ^{225}Ac (**Fig. 2A**; ref. 25). The characterization of the conjugated antibody activity was done utilizing a recently developed immunoreactivity assay (26). First, the conjugation of DOTA to the YS5 antibody was performed in 0.1 mol/L Na_2CO_3/$NaHCO_3$ buffer, followed by SEC purification. The successful conjugation and number of DOTA chelator on YS5 was confirmed with matrix-assisted laser deposition/ionization–time of flight (MALDI-TOF) mass spectroscopy (Supplementary Fig. S2A), which revealed that an average of 8.7 ± 0.2 ($n = 2$) equivalents of DOTA were conjugated to each YS5. The DOTA-YS5 was stored at −20°C until radiolabeling reactions were carried out. The isolated yield of [^{225}Ac]DOTA-YS5 from [^{225}Ac]Ac(NO_3) was 39.4% ± 4.4% ($n = 6$) with a specific activity of 0.10 ± 0.01 μCi per μg of antibody ($n = 6$). As shown in iTLC in **Fig. 2B**, purity of radiolabeled antibody was 94.8% ± 8.1% ($n = 3$). In addition, SEC analysis (Supplementary Fig. S2B) showed no aggregation of the [^{225}Ac]DOTA-YS5 after the labeling and purification process. *In vitro* stability of the radioimmunoconjugate, [^{225}Ac]DOTA-YS5 was evaluated in human serum and saline buffers at 37°C for 14 days. As shown in Supplementary Fig. S2C, >85% of radioimmunoconjugate was intact at all the timepoints except for the 14th day measurement in the saline buffer (~55.24% is intact). The beads-based binding assay (26) results shown in **Fig. 2C** confirm that binding of [^{225}Ac]DOTA-YS5 was 86.4% ± 1.5%, which was reduced to 17.4% ± 0.5% in the blocking sample where 30-fold excess of cold (unlabeled) YS5 was added, and 14.3% ± 1.0% in non–antigen-coated beads. These measurements were performed without waiting for secular equilibrium of the isotope, and similar results were also found after secular equilibrium (Supplementary Fig. S2D). Overall, these results demonstrate that [^{225}Ac]DOTA-YS5 was efficiently radiolabeled with retention of immunoreactivity.

[^{225}Ac]DOTA-YS5 demonstrates binding and cytotoxicity to prostate cancer cells *in vitro*

Next, we studied binding and cytotoxicity of [^{225}Ac]DOTA-YS5 to prostate cancer cells *in vitro*. For binding, 22Rv1 cells incubated with [^{225}Ac]DOTA-YS5 at 7 nmol/L showed 19.25% ± 0.70% binding (Supplementary Fig. S3), which was reduced to 4.46% ± 0.17% by the addition of 2-fold cold YS5. The *in vitro* uptake of [^{225}Ac]DOTA-YS5 was studied on 22Rv1 and DU145 cells. Results in **Fig. 2D** and **E** show number of cell-associated (membrane-bound, internalized, and total) molecules for the cells incubated with [^{225}Ac]DOTA-YS5. Interestingly, the two cell lines used in this study show different binding and internalization patterns. In case of 22Rv1 cells (**Fig. 2D**), most of the [^{225}Ac]DOTA-YS5 was internalized or bound in the first 30 minutes of incubation, whereas the membrane-bound activity increased up to 24 hours. Total cell-associated molecules (membrane-bound + internalized) for 22Rv1 cells at 24 hours were $9.7 \times 10^{11} \pm 4.5 \times 10^{10}$, which suggests that a greater number of [^{225}Ac]DOTA-YS5 molecules were interacting with CD46 on cell surface over time. In contrast, the total number of [^{225}Ac]DOTA-YS5 antibody molecules bound to DU145 cells (**Fig. 2E**) increased from $8.0 \times 10^{10} \pm 7.6 \times 10^9$ at 30 minutes to $4.5 \times 10^{11} \pm 1.9 \times 10^9$ molecules at 24 hours.

The cell-killing activity of [^{225}Ac]DOTA-YS5 was studied with cell viability and clonogenic assays. A dose-dependent reduction in cell viability was observed by the treatment of [^{225}Ac]DOTA-YS5 on 22Rv1 cells (**Fig. 2F**). The IC_{50} of [^{225}Ac]DOTA-YS5 and control nonspecific [^{225}Ac]DOTA-IgG were found to be 80.1 ± 23.5 pCi/mL, and 7.34 ±0.9 nCi/mL, respectively. In the clonogenic assay where tumor cells grow into large colonies, IC_{50} of [^{225}Ac]DOTA-YS5 was determined to be 10.09 ± 3.61 nCi/mL (**Fig. 2G**). These data suggest that [^{225}Ac]DOTA-YS5 has high specific binding and potent cytotoxicity against prostate cancer cells.

In vivo biodistribution, tumor uptake, and autoradiographic analysis of [^{225}Ac]DOTA-YS5

Because imaging of [^{225}Ac]DOTA-YS5 is challenging owing to low emission rate of imageable photons, we utilized *ex vivo* biodistribution studies to assay the tissue distribution of the radiopharmaceutical. Mice bearing 22Rv1 xenografts (PSMA positive, AR positive) were administered 0.5 μCi activity of [^{225}Ac]DOTA-YS5 via tail vein. As shown in **Fig. 3A** and Supplementary Table S2, tumor uptake of [^{225}Ac]DOTA-YS5 at 24 hours (day 1) post injections (p.i.) was 11.64% ± 1.37%ID/g, which kept increasing up to 96 hours (day 4) to 28.58% ± 10.88%ID/g. The average %ID/g for 168 hours (day 7), 264 hours (day 11), and 336 hours (day 14) were found to be 29.35 ± 7.76, 18.10 ± 8.12, and 21.12 ± 12.30, respectively (**Fig. 3A**). Similarly, the last observation on 408 hours p.i (day 17) showed uptake of 31.78% ± 5.89%ID/g. The %ID/g for tumors was higher than nontargeted organs for all timepoints, except 24 hours, where a high uptake was seen in kidneys. Tumor to blood, tumor to kidney, and tumor to muscle ratios (**Fig. 3B**; Supplementary Table S3) increased from day 1 to day 17, suggesting the clearance of the [^{225}Ac]DOTA-YS5 in most of the organs including muscle and kidneys, with simultaneous accumulation in tumor tissue. As seen from gamma energy spectra in **Fig. 3C** and Supplementary Fig. S4, the higher uptake seen in kidneys at 24 hours could be due to the accumulation of ^{213}Bi (from ^{225}Ac decay)

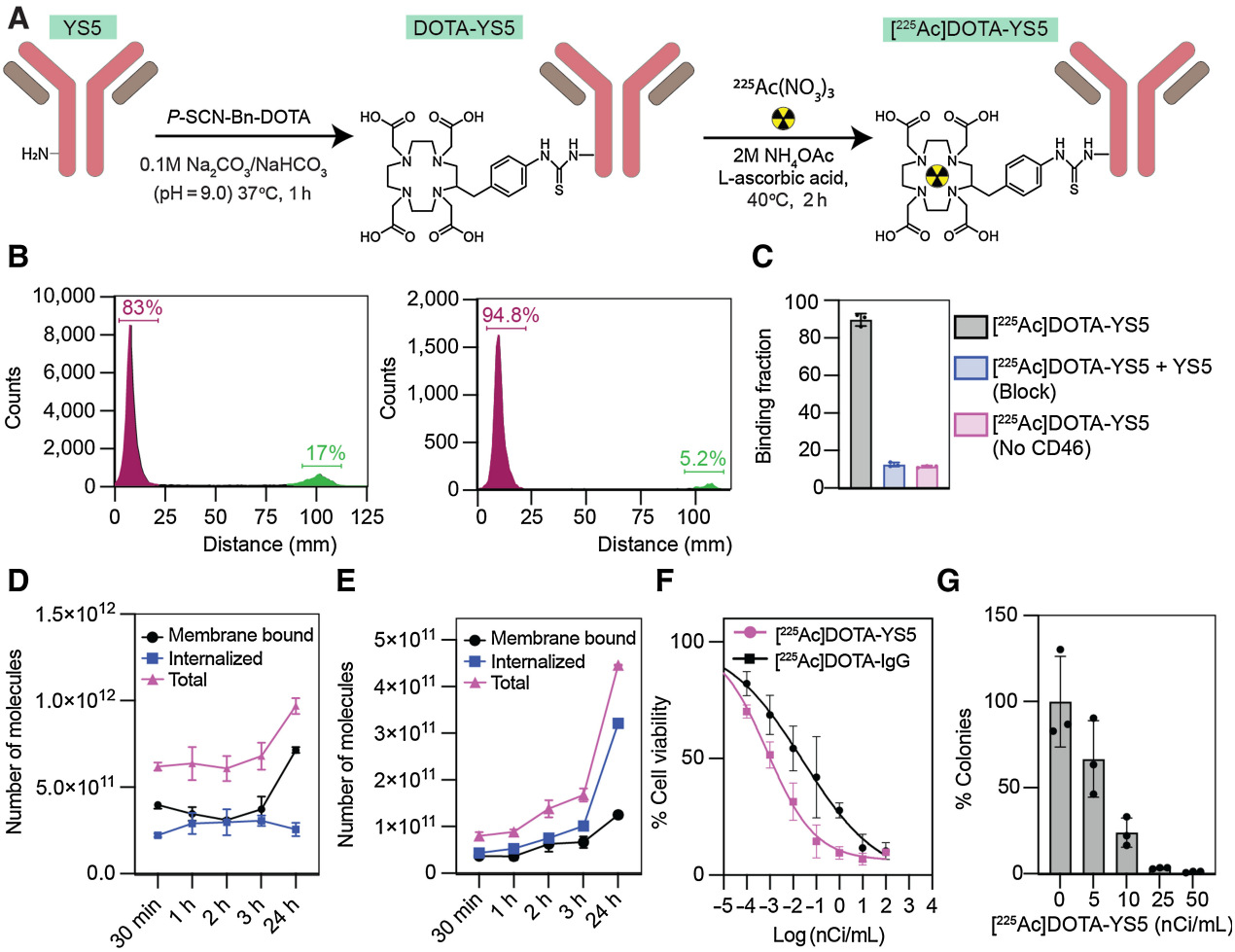

Figure 2.

Preparation and confirmation of retention of immunogenicity of the [^{225}Ac]DOTA-YS5 by *in vitro* studies. **A,** Synthesis scheme of [^{225}Ac]DOTA-YS5. **B,** iTLC plots of the crude reaction and the purified [^{225}Ac]DOTA-YS5 showing 94.84% ± 8.1% ($n = 3$) purity. **C,** Magnetic beads assay showing 86.4% ± 1.5% binding of [^{225}Ac]DOTA-YS5 denoting the preservation of immunogenicity of radiolabeled antibody. The addition of cold YS5 reduces binding to 17.4% ± 0.5%, demonstrating specificity (data represented as mean ± SD, $n = 4$). Cell-associated molecules of [^{225}Ac]DOTA-YS5 in 22Rv1 (**D**) and DU145 (**E**) cells after the treatment for different timepoints. **F,** MTT assay showing dose-dependent reduction of cell viability from [^{225}Ac]DOTA-YS5 treatment on 22Rv1 cells (IC_{50}: 80.0 ± 20.0 pCi/mL for [^{225}Ac]DOTA-YS5 and 7.3 ± 0.9 nCi/mL for [^{225}Ac]DOTA-IgG). **G,** Clonogenic survival of the 22Rv1 cells treated with [^{225}Ac]DOTA-YS5 showed a dose-dependent decrease in the number of colonies after treatment ($n = 3$).

in the kidneys, a phenomenon that has been reported by others (27, 28). This was not observed in other tissues, including the bones (Supplementary Fig. S4). The reduction in activity of blood from 24 hours (11.64 ± 1.37%ID/g) to 408 hours (1.71 ± 0.47%ID/g) indicates gradual clearance via liver and kidney (**Fig. 3A**).

Supplementary Figure S5 shows dosimetry analysis from the biodistribution studies. Dosimetric analysis was performed by considering ^{225}Ac as a dominant emitter of alpha particles and primary contributor for therapeutic effect; the daughter isotopes were not included in the calculations because there is an uncertainty that all daughters stay at the same site and the dose contributions are minor compared with that from alpha emission of ^{225}Ac. The tumor with an average weight of 0.5 g received an average 37 Sv of equivalent dose with 0.5 μCi injections of [^{225}Ac]DOTA-YS5. The highest amount was delivered to tumor tissue, suggesting the potential of antitumor response from [^{225}Ac]DOTA-YS5. In addition, normal healthy organs, including bone, kidneys, stomach, and heart, are exposed to high doses (roughly 5 Sv or higher; Supplementary Fig. S5).

Digital autoradiographic imaging (iQID camera) was performed to study tissue distribution of [^{225}Ac]DOTA-YS5 in tumor and mouse organs. **Figure 3D** shows iQID camera digital autoradiographs for organs collected on day 1, day 2, day 4, and day 7 after injections of [^{225}Ac]DOTA-YS5. Signal from [^{225}Ac]DOTA-YS5 was not uniform in tumor tissues (**Fig. 3D**). For the remaining organs, distribution of [^{225}Ac]DOTA-YS5 was homogenous.

[^{225}Ac]DOTA-YS5 treatment induces DNA double-strand breaks in tumor tissue

As shown in **Fig. 4**, the 22Rv1 xenografts treated with 0.5 μCi activity of [^{225}Ac]DOTA-YS5 were stained with hematoxylin and eosin (H&E) and a DNA damage marker protein (phosphorylated γ-H2AX). **Figure 4A** and **B** shows that treatment of 0.5 μCi activity dose of the [^{225}Ac]DOTA-YS5 for day 7 or day 14 increases the

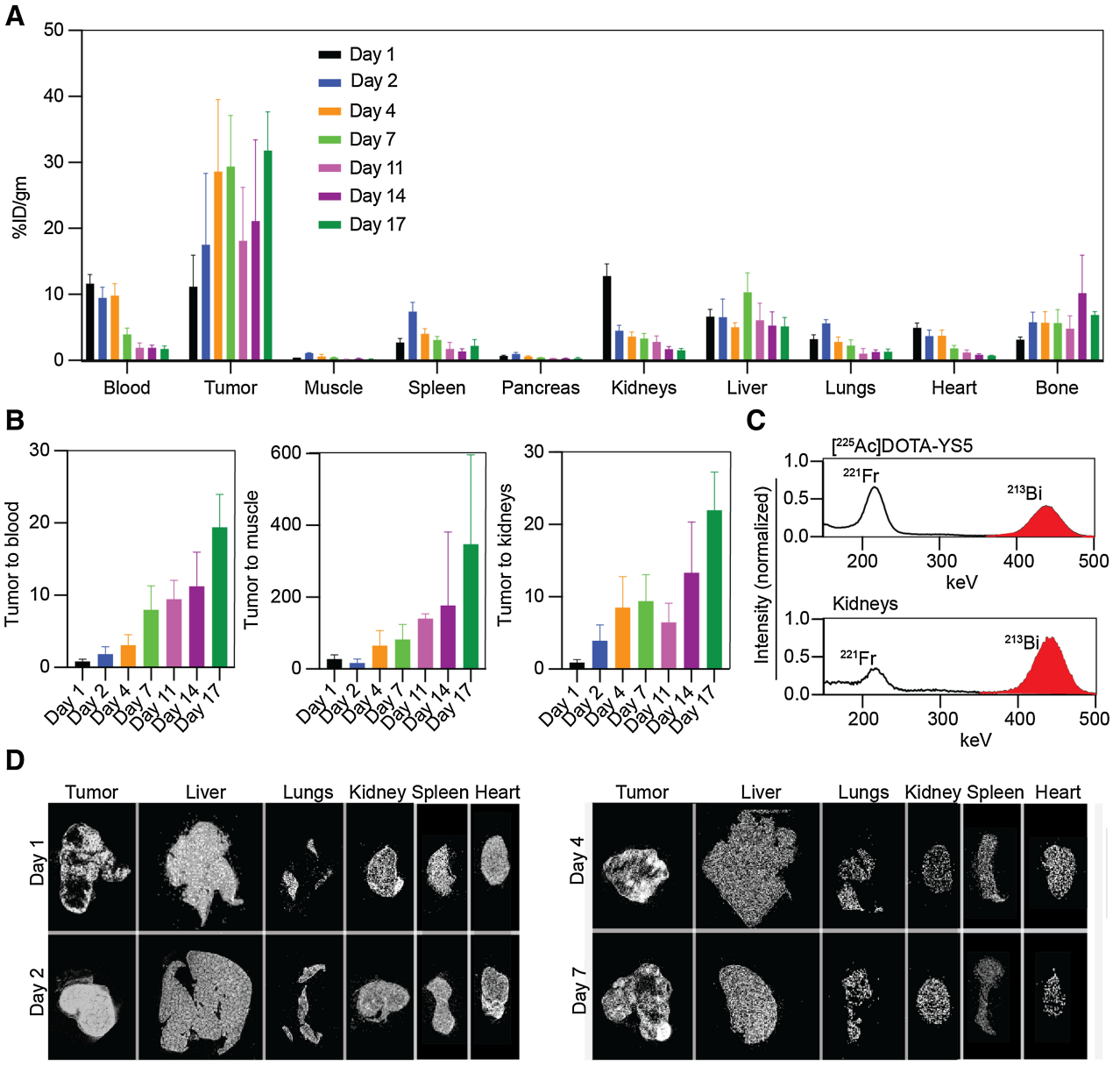

Figure 3.

Biodistribution of the [^{225}Ac]DOTA-YS5 in 22Rv1 xenograft-bearing mice confirming high delivery of the [^{225}Ac]DOTA-YS5 to tumor tissue. **A,** The distribution of [^{225}Ac]DOTA-YS5 (represented as %ID/g, mean ± SD, $n = 4$) in organs collected from day 1 to day 17. **B,** Tumor to blood, tumor to muscle, and tumor to kidney ratios from the biodistribution studies indicate [^{225}Ac]DOTA-YS5 clearance with simultaneous accumulation in tumor tissue. **C,** Gamma energy spectra showing accumulation of ^{213}Bi in kidneys. As compared with the equilibrium gamma energy spectra of [^{225}Ac]DOTA-YS5, increased intensity of the ^{213}Bi was observed in kidney samples at 24 hours. **D,** iQID camera digital autoradiographic imaging for distribution of the [^{225}Ac]DOTA-YS5 in 22Rv1 xenograft tumor and healthy tissues studied from day 1 to day 7 after injections. The distribution of the radioactivity in tumor tissue is heterogenous, whereas all the other organs show homogenous distribution.

γ-H2AX foci in the cell nucleus confirming DNA double-strand breaks. The number of γ-H2AX foci per cell in 7 days treatment of 0.5 μCi activity doses were found to be 4.46 ± 0.75, significantly higher than saline (1.37 ± 0.10 foci per cell, *P* value, 0.02; **Fig. 4A**; Supplementary Fig. S6). Similarly, as shown in **Fig. 4B** and Supplementary Fig. S6, a higher number of the γ-H2AX foci (4.90 ± 0.55 per cell) were also observed for 14 days p.i. of [^{225}Ac]DOTA-YS5 (*P* value, 0.02). In addition, DAPI and H&E staining for the tumors from [^{225}Ac]DOTA-YS5 14 days after treatment (**Fig. 4B**), showed deformed and pycnotic nuclei confirming high nuclear damage. To further investigate the [^{225}Ac]DOTA-YS5 uptake and DNA damage response, H&E staining as well as CD46 and γ-H2AX staining of the tumor was correlated with the digital autoradiographs. The results for tumor tissues stained on day 1, day 2, day 4, and day 7 after treatment (Supplementary Fig. S7) show that CD46 was homogeneously expressed, with the exception of some areas of central necrosis visualized on H&E stain. These areas of

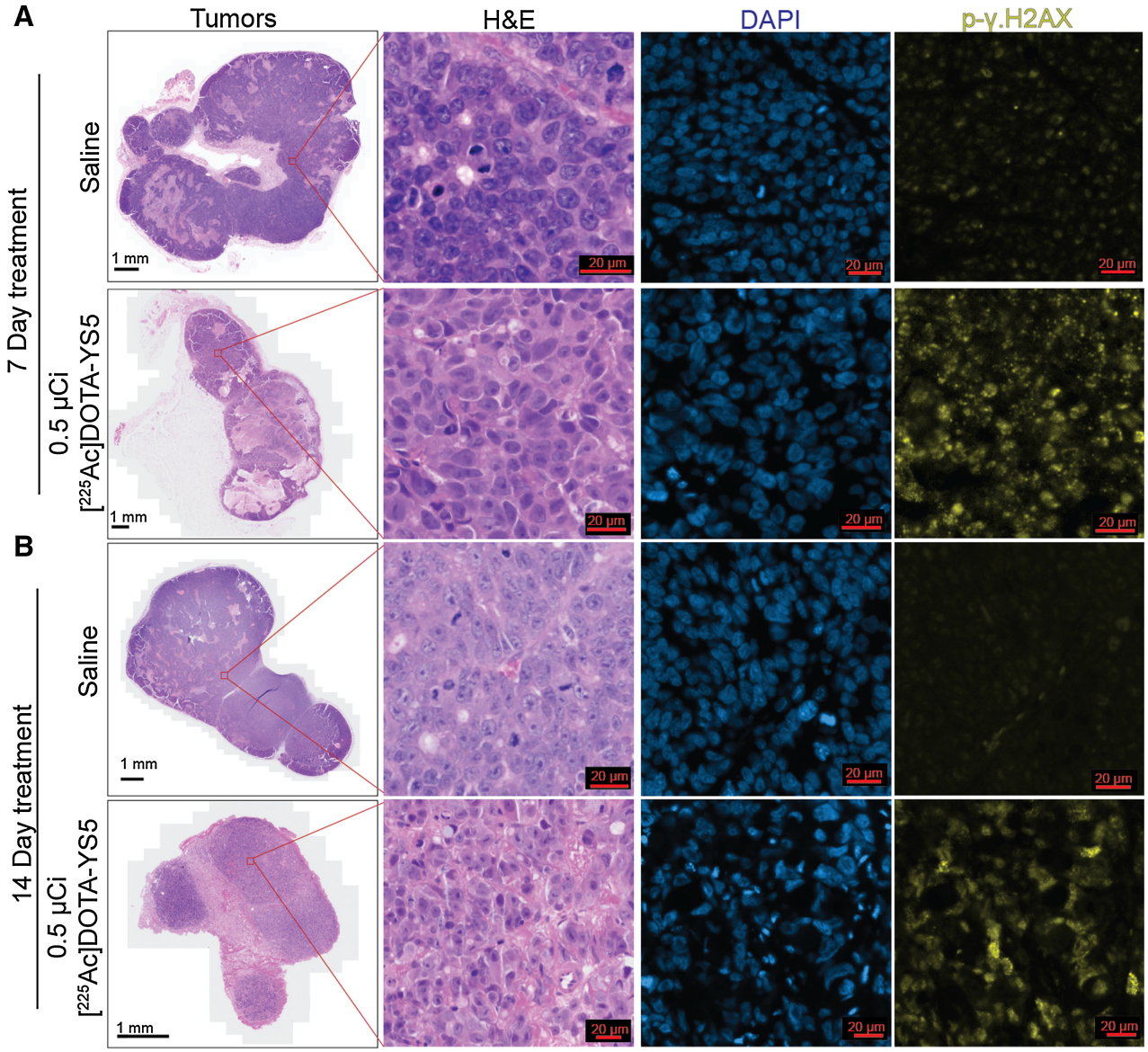

Figure 4.

Histology and immunofluorescence imaging showing DNA damage after [^{225}Ac]DOTA-YS5 treatment. H&E and phosphorylated γ-H2AX (p-γ.H2AX) staining confirms morphologic changes and p-γ.H2AX foci for [^{225}Ac]DOTA-YS5 treatment for 7 days (**A**) and 14 days (**B**; $n = 2$).

necrosis also demonstrated reduced uptake of [^{225}Ac]DOTA-YS5 on the autoradiography. In general, γ-H2AX foci colocalized with CD46 expression.

Toxicity and MTD

Initial acute toxicity studies were carried out for 15 days in male nude mice (without tumor) injected with saline, 0.06, 0.125, 0.25, or 0.5 μCi of [^{225}Ac]DOTA-YS5. Bodyweight measurements shown in Supplementary Fig. S8A indicate no significant weight loss in [^{225}Ac]DOTA-YS5–treated mice for 15 days. Following the 15 days of observation, mice in these groups were euthanized for further evaluation. The liver and kidney function test results shown in Supplementary Fig. S8B and Supplementary Table S4 demonstrate no significant difference in saline versus treated groups. Along with the liver and kidney function test, complete blood count measurements also showed no significant changes in the blood cell counts for saline versus treated groups (Supplementary Fig. S8C; Supplementary Table S5). Histologic evaluation of the organs collected after 15 days showed no significant changes in the saline versus treated groups.

Following the acute toxicity studies, chronic toxicity studies were performed (**Fig. 5**; Supplementary Tables S6 and S7). The male nude mice were injected with saline, 0.25, 0.5, or 1 μCi of [^{225}Ac]DOTA-YS5 and were observed for 117 days for any sign of illness, pain, and body weight loss. All the mice in 1 μCi treatment group were euthanized on 14th day p.i. due to significant toxicity and body weight loss (**Fig. 5A**). Out of 4 animals in the 0.5 μCi group, a significant body weight loss was observed, and 1 mouse was euthanized on day 103 due to body weight loss by 20%, while the saline and 0.25 μCi groups demonstrated no

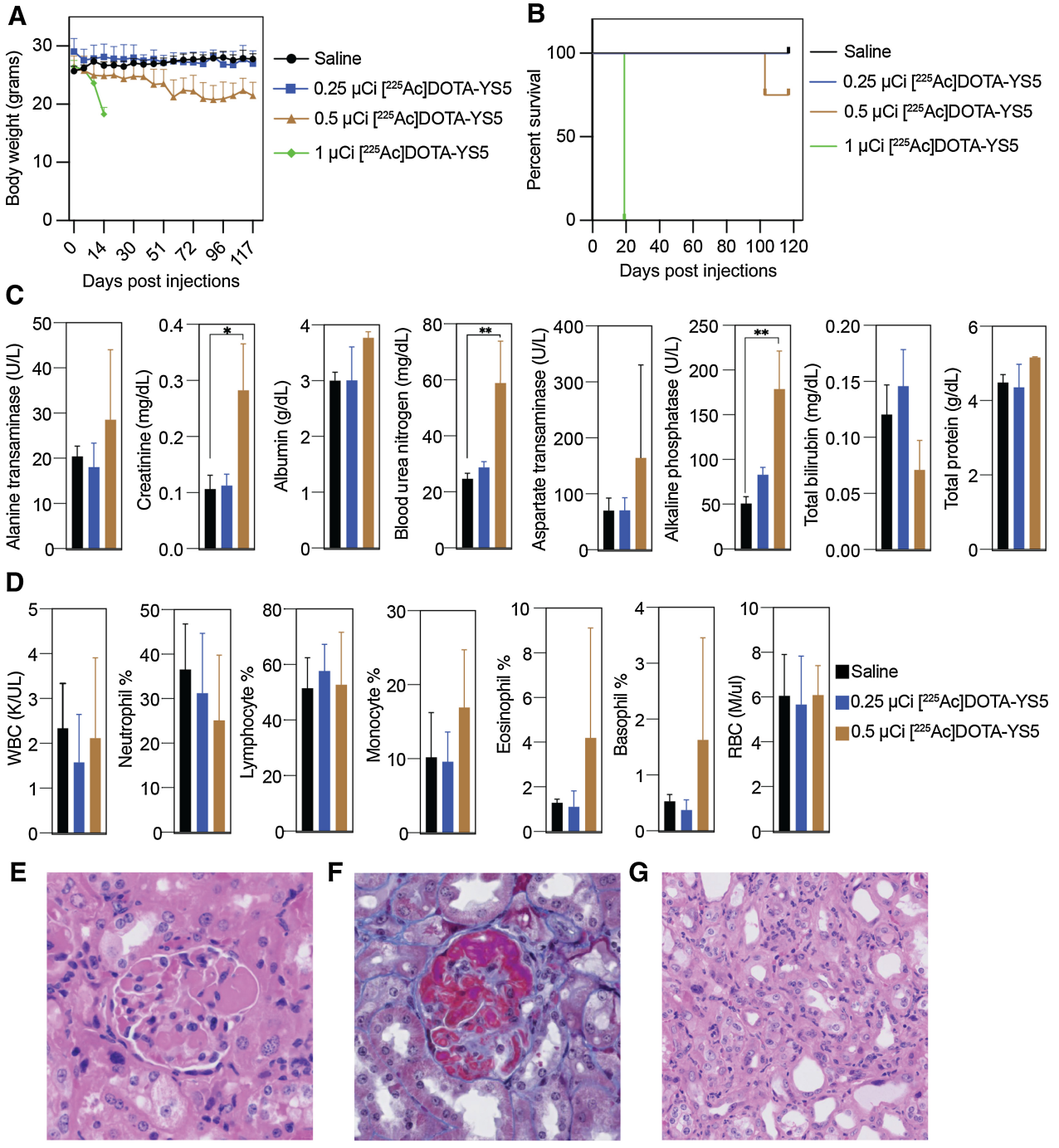

Figure 5.

Chronic toxicity study of the [^{225}Ac]DOTA-YS5 in nude mice ($n = 4$). **A,** The body weight measurements of the mice injected with the [^{225}Ac]DOTA-YS5 show a gradual decrease with 0.5 µCi administration, whereas no significant body weight loss was seen in the 0.25 µCi dose or in the saline control group. **B,** Survival plot in the toxicity study. **C,** Liver and kidney function tests results showing increase in creatinine, blood urea nitrogen, and alkaline phosphatase. **D,** Blood cell counts confirming no significant difference in saline control versus [^{225}Ac]DOTA-YS5–injected mice. **E,** Histologic H&E findings in the kidney of a mouse injected with 0.5 µCi activity level with diffuse parenchymal damage and occlusion of glomerular capillary loops by fibrin thrombi with glomerulosclerosis. **F,** Trichrome stain highlighting fibrin thrombi. **G,** Higher power images showing tubular injury in the mouse treated with [^{225}Ac]DOTA-YS5. One-way ANOVA P values are indicated as *, $P < 0.05$; **, $P < 0.01$; ***, $P < 0.001$.

detectable body weight loss (**Fig. 5A** and **B**). On laboratory analysis, creatine and blood urea nitrogen levels were elevated at 0.5 μCi activity level (**Fig. 5C**; Supplementary Table S6), consistent with renal toxicity. Alkaline phosphatase levels (for liver or bone damage) were also higher in 0.5 μCi treatment (**Fig. 5C**), while the liver function tests for alanine transaminase and aspartate transaminase were unchanged. There were no significant changes in blood counts for saline versus treated groups (**Fig. 5D**; Supplementary Table S7).

Histologic evaluation of the organs collected in this chronic toxicity study revealed that 0.5 μCi resulted in significant renal damage. As shown in **Fig. 5E–G**, for the 0.5 μCi activity level, glomeruli demonstrated marked fibrin deposition in the capillary loops and glomerulosclerosis (**Fig. 5E** and **F**). In addition, the renal tubules showed dilatation and flattening with scattered cells containing enlarged nuclei with anisonucleosis and necrotic luminal epithelial cells (**Fig. 5G**). Other organs including spleen, bone and bone marrow, lungs, heart, and liver showed no histologic evidence of damage (Supplementary Fig. S9).

[^{225}Ac]DOTA-YS5 is effective in reducing tumor volume and prolonging survival in cell line–derived prostate cancer models

CD46-expressing cell line–derived prostate cancer xenograft models were used to study therapeutic efficacy of [^{225}Ac]DOTA-YS5. Cohorts of $n = 7$ 22Rv1 xenograft (PSMA-positive)-bearing mice were randomized to injection with saline, 0.25 or 0.5 μCi activity levels of [^{225}Ac]DOTA-YS5, or 0.5 μCi of [^{225}Ac]DOTA-IgG. Nontargeting [^{225}Ac]DOTA-IgG was kept as a negative control test to assay for nonspecific treatment effects. As shown in **Fig. 6A**, treatment with 0.25 and 0.5 μCi of [^{225}Ac]DOTA-YS5 significantly inhibited tumor growth in an activity-dependent manner, while mice in control cohorts (saline

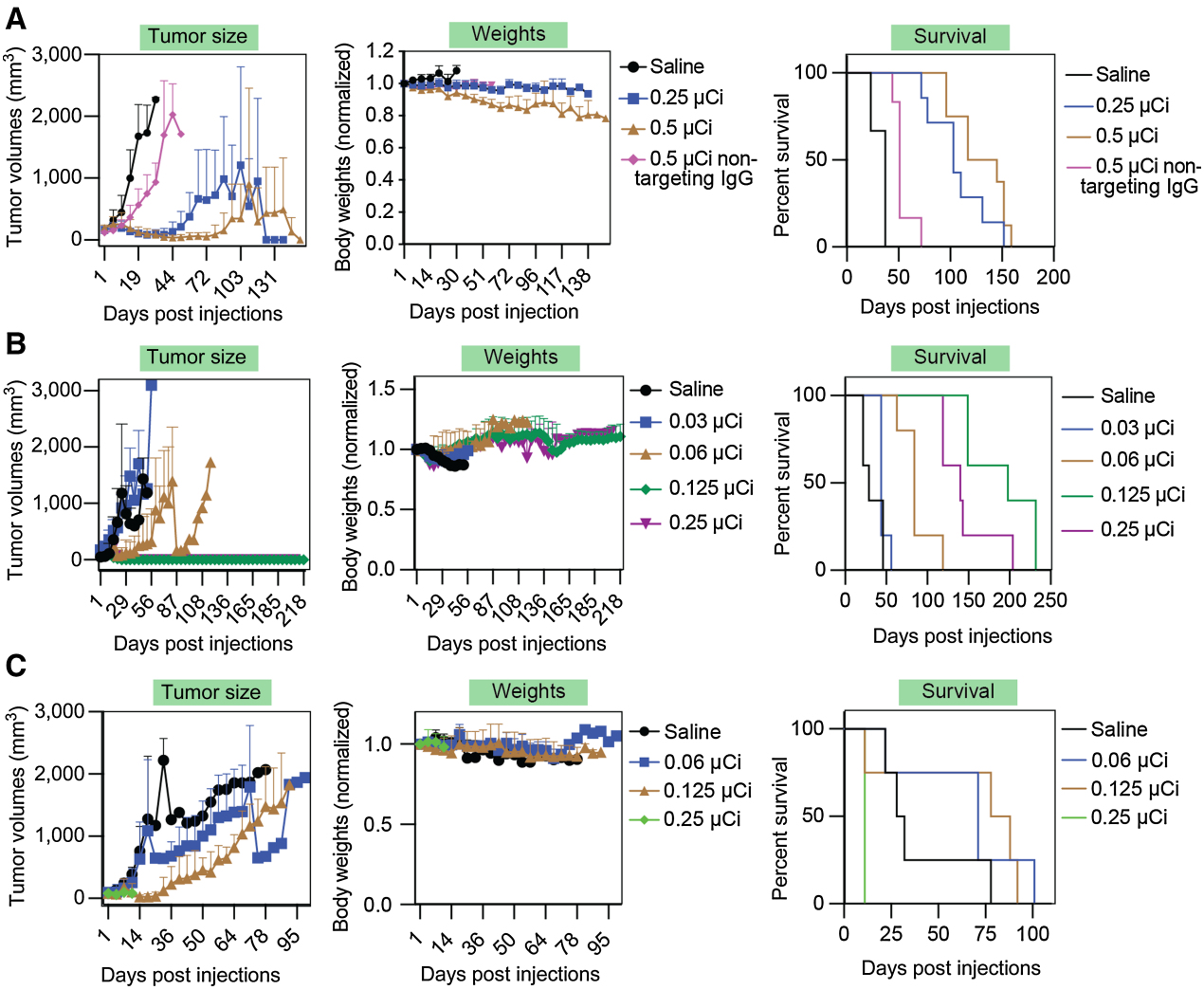

Figure 6.

Antitumor activity of [^{225}Ac]DOTA-YS5 in subcutaneous 22Rv1 and PDX tumor models. **A,** Effect of [^{225}Ac]DOTA-YS5 in 22Rv1 tumor-bearing mice ($n = 7$). Tumor volume measurements demonstrated delayed 22Rv1 tumor growth in 0.25 and 0.5 μCi dose groups of [^{225}Ac]DOTA-YS5. Average body weights of the mice indicated gradual body weight loss in the 0.5 μCi treatment group. Kaplan–Meier survival plot showing improved survival probability of the [^{225}Ac]DOTA-YS5–treated 22Rv1 xenograft-bearing mice compared against control groups. **B,** Effect of [^{225}Ac]DOTA-YS5 in LTL-545 PDX. Tumor volumes, average body weights, and overall survival in the animals administered with [^{225}Ac]DOTA-YS5 at 0.03, 0.06, 0.125, and 0.25 μCi dose treatment ($n = 5$). **C,** Tumor size, overall survival, and body weight for the LTL-484 PDX mice treated with [^{225}Ac]DOTA-YS5 ($n = 4$). Data represented as mean ± SD.

and [^{225}Ac]DOTA-IgG) showed rapid tumor growth. The survival plot (**Fig. 6A**) indicates that median survival of the mice treated with saline and [^{225}Ac]DOTA-IgG were 37 and 51 days ($P = 0.0012$), respectively. In contrast, the median survival of 0.25 and 0.5 μCi groups of [^{225}Ac]DOTA-YS5 was significantly improved to 103 ($P = 0.0006$) and 131 days ($P = 0.0003$), respectively. The body weight measurements of the mice in these groups are shown in **Fig. 6A**; results indicate that a 0.5 μCi dose of [^{225}Ac]DOTA-YS5 results in a gradual decrease in body weights over the period, consistent with the toxicity studies. **Figure 6A** shows that 0.5 μCi dose of [^{225}Ac]DOTA-YS5 has the highest antitumor response but also greater toxicity. Overall, these data demonstrate that 0.25 and 0.5 μCi doses of [^{225}Ac]DOTA-YS5 are effective for treatment of 22Rv1 xenografts, with toxicity observed at the 0.5 μCi activity level.

We also tested a fractionated therapy regimen to further evaluate the treatment efficacy of [^{225}Ac]DOTA-YS5. We administered fractionated dose (three doses) of 0.125 μCi of [^{225}Ac]DOTA-YS5 to the mice with 22Rv1 xenografts on day 1, day 37, and day 49. As shown in Supplementary Fig. S10, the three fractionated administrations of 0.125 μCi of [^{225}Ac]DOTA-YS5 delayed tumor growth significantly compared with the saline control group. The median survival of the saline group (17 days) was significantly lower than the study group treated with three doses of 0.125 μCi (71.5 days, $P = 0.0002$) of [^{225}Ac]DOTA-YS5 (Supplementary Fig. S10). Out of the 10 mice in the fractionated dose group (0.125 μCi), no mouse was euthanized because of body weight loss, while only 3 mice showed a transient 15% body weight loss (Supplementary Fig. S10), and all mice regained their body weights. These data suggest that a fractionated therapy approach represents a potential method for treatment utilizing [^{225}Ac]DOTA-YS5.

In addition, a CD46-positive, PSMA-negative, AR-negative prostate cancer cell line–derived xenograft model (DU145) was also employed to study the effect of [^{225}Ac]DOTA-YS5. As shown in Supplementary Fig. S11, 0.25 and 0.5 μCi dose of [^{225}Ac]DOTA-YS5 had an antitumor effect that delayed the tumor growth. Saline-treated mice showed 5-fold tumor growth in 44 days, while similar tumor growth was seen in 124 days for 0.125 μCi activity treatment. In fact, the 0.5 μCi dose showed tumor growth inhibition as soon as day 5 of the injections, and all mice from this group showed complete response. However, due to the indolent growth of the tumors in the control group in this study, an overall survival benefit was not observed (Supplementary Fig. S11).

Antitumor effect of [^{225}Ac]DOTA-YS5 in PDX models

We next evaluated antitumor potential of the [^{225}Ac]DOTA-YS5 in PDX models. CD46-overexpressing PDXs were used for studying the therapeutic efficiency of the [^{225}Ac]DOTA-YS5. The PSMA-negative neuroendocrine prostate cancer PDX, LTL-545–bearing mice were injected with saline, 0.03, 0.06, 0.125, and 0.25 μCi dose of [^{225}Ac]DOTA-YS5 (**Fig. 6B**). As shown in tumor volume plot (**Fig. 6B**), all the mice from 0.125 and 0.25 μCi groups demonstrated complete resolution of the tumor, whereas 0.06 μCi delayed the tumor growth as compared with saline control. Median survival of the animals treated with saline, 0.03, 0.06, 0.125, and 0.25 μCi were found to be 29, 44 (not statistically significant), 84 ($P = 0.0025$), 198 ($P = 0.0025$), and 140 days ($P = 0.0025$), respectively (**Fig. 6B**). During the first 15 days of treatment (**Fig. 6B**), the body weights of LTL-545–bearing mice treated with [^{225}Ac]DOTA-YS5 decreased, but these mice gradually regained their body weights.

NSG mice bearing LTL-484 PDX (CD46 and PSMA positive) were randomized into four arms for saline and [^{225}Ac]DOTA-YS5 injections (0.06, 0.125, and 0.25 μCi; **Fig. 6C**). The 0.25 μCi dose injected mice demonstrated acute toxicity manifested by hunched posture and reduced locomotion on 11th day p.i. On the other hand, we found that that 0.06 (median survival = 71, $P = 0.335$) and 0.125 μCi (median survival = 83, $P = 0.169$) dose delayed the tumor growth with a nonstatistically significant trend toward increase in the median survival as compared with saline control (median survival = 30). The NSG mice used in these experiments were more sensitive to radiation dose compared with nude mice used for the cell line–derived xenograft studies, with a constant decrease in body weight seen over the period of treatment (**Fig. 6C**; ref. 29).

Discussion

Alpha-particle therapies hold great potential for treating metastatic prostate cancer. The PSMA-targeted alpha-particle therapy ([^{225}Ac-PSMA-617) showed potential antitumor response but with considerable toxicities (19, 30). Recently, several studies have acknowledged the issue of less or no expression of PSMA in advanced prostate tumors which could result in resistance to PSMA-directed therapies (31). Our prior report taken together with new data (**Fig. 1**) showed that anti-CD46 antibody (YS5)-based radiotracer probe ([^{89}Zr]DFO-YS5) successfully targeted the overexpression of CD46 on prostate cancer cell surface for PET imaging, including in PSMA-negative models (17). Inspired by these results as well as prior studies demonstrating efficacy of the YS5 antibody as an antibody–drug conjugate, we hypothesized that the YS5 antibody would serve as an ideal targeting vector for delivery of therapeutic alpha particles (14).

We report the CD46-targeted alpha-particle therapy with [^{225}Ac]DOTA-YS5 for PSMA-positive and PSMA-negative tumors. We developed a reproducible radiosynthesis and found that [^{225}Ac]DOTA-YS5 was able to target protein CD46 *in vitro* and *in vivo*. In a biodistribution study, high tumor uptake of [^{225}Ac]DOTA-YS5 was observed over 17 days, along with clearance from healthy organs. We noted all the healthy organs except liver and bones demonstrated gradual clearance of [^{225}Ac]DOTA-YS5. The steady uptake in liver corroborates with previous studies reported for ^{225}Ac-labeled PSMA-targeting antibodies (32). Similar results for liver were also noted in earlier studies with [^{89}Zr]DFO-YS5 over the period of 168 hours (17). Favorable tumor to blood and tumor to muscle ratios were found, suggesting feasibility for therapeutic studies.

We conducted a detailed toxicologic analysis following treatment, with the key finding of dose-limiting nephrotoxicity. Our data suggest that this is due at least in part to non–target-mediated redistribution of the daughter isotope, ^{213}Bi. Though an antibody-chelate may retain the ^{225}Ac, as the time passes ^{225}Ac decays into daughter isotopes ^{213}Bi and ^{221}Fr which are ejected from the chelator due to the recoil effect. These daughter isotopes are reported to accumulate in kidneys, resulting in off-target toxicity (28). Our observations from the gamma-ray spectra of ^{213}Bi and ^{221}Fr confirm that there is a nonhomogenous distribution of daughter nuclei in mouse organs. Specifically, comparison of gamma spectra between organs in Supplementary Fig. S4 shows increased ^{213}Bi peak intensity and therefore ^{213}Bi accumulation in kidneys. In addition, histopathology analysis reveals that ^{213}Bi accumulation results in renal parenchymal damage, fibrin thrombi formation, and glomerulosclerosis. We conducted a dosimetry estimation, neglecting the daughter ^{213}Bi, which did not demonstrate disproportionate renal radiation dose, further supporting our hypothesis that redistribution plays a key role (Supplementary Fig. S5). This substantiates the previous finding of ^{213}Bi accumulation in kidneys resulting in kidney toxicity. Unexpectedly, we have also observed uptake of [^{225}Ac]DOTA-YS5 in bone, but no damage to bone marrow

or hematologic toxicity was seen, possibly due to the short range and low penetrability of alpha particles. Given that the YS5 antibody does not bind to mouse CD46 protein, the toxicity study results should be interpreted with caution, as we may underestimate the toxicity profile in humans. In addition, the toxicity of [^{225}Ac]DOTA-YS5 may not be comparable with the ^{225}Ac-PSMA-617, owing to its high molecular weight, different clearance route, and increased blood half-life.

Evaluation of therapeutic efficiency revealed that [^{225}Ac]DOTA-YS5 shows a significant antitumor response across a panel of prostate cancer models, including in 22Rv1 (weakly PSMA-positive) and DU145 (PSMA-negative), as well as the LTL-545 (PSMA-negative neuroendocrine) and LTL-484 (PSMA-positive adenocarcinoma) PDX models. Marked increases in overall survival were observed in the 22Rv1 and LTL-545 models, with the latter demonstrating complete eradication of the tumor at the higher dose levels with no evidence of recovery even at delayed timepoints. Considering the long period of therapeutic efficiency studies, 0.25 μCi was the MTD in the nu/nu model, with a prominent antitumor response. In the highly radiosensitive NSG model (required to grow the PDX models), the MTD is at a lower dose (0.125 μCi activity) with significant antitumor effects and an increase in survival.

Apart from PSMA, potential targets for prostate cancer for radiopharmaceutical therapy include prostate stem cell antigen (PSCA), delta-like ligand 3 (DLL3), kallikrein 2 (hK2), and CUB domain-containing protein 1 (CDCP1; refs. 20, 33–35). When evaluated in preclinical imaging and therapy studies, these agents show promising results. Our results demonstrate that CD46 targeting with [^{225}Ac]DOTA-YS5 could deliver the radiopharmaceutical to a broader range of prostate cancers compared with PSMA targeting. This could be further evaluated in a detailed study of CD46 expression across a panel of PDXs and potentially patient biopsy samples.

Feasibility of translation of [^{225}Ac]DOTA-YS5 to the clinic is high. We discovered that CD46 is an excellent target for mCRPC across differentiation patterns, developed a human antibody YS5 that binds to a tumor-selective conformational epitope, and constructed a YS5-based ADC (14), which is in multiple clinical trials (NCT03575819 and NCT05011188). In addition, we recently developed a YS5-based PET agent (17), which is now in a first-in-human study in patients with mCRPC (NCT05245006). Thus, there is an established path for YS5-based agents to move from the bench to the clinic.

Safety is a critical issue that needs to be carefully investigated. One potential limitation of our study is selection of only two timepoints for toxicity analysis. Future studies will investigate multiple timepoints for acute and chronic toxicity. While ^{225}Ac-antibodies have demonstrated great efficacy, prior studies have also revealed dose-dependent toxicity (21, 36). Potential mechanisms for toxicity include redistribution of the daughter isotopes away from the original site, due to the "recoil" effect (37, 38). We observed this effect in higher uptake of ^{213}Bi in the kidney compared with the other organs. Our results are consistent with prior literature which demonstrates both remarkable efficacy but also toxicity for treating cancer with ^{225}Ac radiopharmaceutical therapy. Moreover, dosimetric analysis of the biodistribution data revealed higher apparent radiation doses to some tissues including bone, kidneys, stomach, and heart. Despite this finding, the only detectable toxicity in our study was to the kidneys. There are several potential routes to mitigate this toxicity, including dose reduction or fractionation, chelation therapy, linker optimization, pretargeting, or the use of alternative isotopes such as ^{177}Lu or ^{212}Pb (39–42).

In conclusion, we have prepared and developed [^{225}Ac]DOTA-YS5 as a RIT agent for the treatment of prostate cancer, which shows efficacy for both PMSA-deficient and PSMA-positive tumors. Because of the CD46-targeting nature of [^{225}Ac]DOTA-YS5, we were able to deliver a high amount of radiation dose to tumor tissue, resulting in a potent antitumor effect. The data presented here provide strong evidence of therapeutic efficacy of [^{225}Ac]DOTA-YS5 in preclinical models, and support future clinical translation of CD46-targeted radioligand therapy.

Authors' Disclosures

D. Beckford-Vera reports other support from Actinium Pharmaceuticals outside the submitted work. Y. Su reports a patent for US20170362330A1 issued, licensed, and with royalties paid from Fortis Therapeutics. J. He reports grants from NCI during the conduct of the study; in addition, J. He holds equity in Molecular Imaging and Therapeutics, Inc., which was converted to equity of Fortis Therapeutics that licensed intellectual properties from the University of California. R. Aggarwal reports grants from Fortis Therapeutics during the conduct of the study. R. Aggarwal also reports grants from Janssen; grants and personal fees from Merck, AstraZeneca, and Novartis; and personal fees from Bioexcel Therapeutics, EcoR1, Dendreon, Tersara, Targeted Oncology, OncLive, Lumanity, Exelixis, PCCTC, Jubliant Therapeutics, Modra Therapeutics, SNMMI, and Bayer outside the submitted work. H.F. VanBrocklin reports grants from CDMRP Department of Defense and UCSF PICT program funded by NIH P30 during the conduct of the study. Y. Seo is equity holder of Molecular Imaging and Therapeutics, Inc., which was converted to equity of Fortis Therapeutics that licensed intellectual properties from the University of California. J. Chou reports grants from Department of Defense Prostate Cancer Research Program, NIH/NCI K08CA273514, and Prostate Cancer Foundation, as well as personal fees from Exai Bio outside the submitted work. B. Liu reports grants from NIH during the conduct of the study, and is a founder/board member of Fortis Therapeutics. In addition, B. Liu has a patent for US20140271685A1 issued, licensed, and with royalties paid from Fortis Therapeutics; a patent for US20170362330A1 issued, licensed, and with royalties paid from Fortis Therapeutics; and a patent for US8865873B2 issued, licensed, and with royalties paid from Fortis Therapeutics. R.R. Flavell reports grants from U.S. Department of Defense and NIH during the conduct of the study; in addition, R.R. Flavell has a patent on the development of new chelators for alpha-radiotherapy, not related directly to this work. No disclosures were reported by the other authors.

Authors' Contributions

A.P. Bidkar: Data curation, software, formal analysis, investigation, visualization, methodology, writing–original draft, writing–review and editing. **S. Wang:** Data curation, formal analysis, investigation, methodology. **K.N. Bobba:** Data curation, investigation, methodology. **E. Chan:** Resources, data curation, methodology. **S. Bidlingmaier:** Resources, methodology. **E.A. Egusa:** Data curation, visualization. **R. Peter:** Software, formal analysis. **U. Ali:** Resources, data curation. **N. Meher:** Data curation, software, formal analysis, methodology. **A. Wadhwa:** Investigation, visualization. **S. Dhrona:** Validation. **C. Dasari:** Visualization. **D. Beckford-Vera:** Formal analysis, methodology. **Y. Su:** Formal analysis, methodology. **R. Tang:** Formal analysis, investigation. **L. Zhang:** Data curation, formal analysis. **J. He:** Formal analysis, supervision, validation, methodology. **D.M. Wilson:** Conceptualization, resources, data curation, supervision. **R. Aggarwal:** Conceptualization, resources, formal analysis, supervision, methodology. **H.F. VanBrocklin:** Conceptualization, resources, data curation, supervision, methodology. **Y. Seo:** Conceptualization, resources, supervision, investigation, methodology. **J. Chou:** Conceptualization, resources, data curation, formal analysis, methodology. **B. Liu:** Conceptualization, resources, data curation, software, formal analysis, supervision, funding acquisition, validation, investigation, methodology, writing–original draft, project administration, writing–review and editing. **R.R. Flavell:** Conceptualization, resources, data curation, software, formal analysis, supervision, funding acquisition, validation, investigation, methodology, writing–original draft, project administration, writing–review and editing.

Acknowledgments

R.R. Flavell acknowledges funding from Translational Science awards from the Prostate Cancer Research Program of the Congressionally Directed Medical Research Program of the U.S. Department of Defense (W81XWH-21-1-0792, W81XWH-20-1-0292), pilot funding through the UCSF Precision Imaging of Cancer and Therapy Program, and pilot funding through the UCSF Cancer Imaging Resource and Preclinical Therapeutics Core through P30CA082103. ^{225}Ac was supplied by the

U.S. Department of Energy Isotope Program, managed by the Office of Isotope R&D and Production. MALDI-MS data were provided by the Mass Spectrometry Facility, Department of Chemistry, University of Alberta (Edmonton, Alberta, Canada). Blood cell counts and organ function tests were performed by Comparative Pathology Laboratory, UC Davis School of Veterinary Medicine. Histology staining procedures were carried out by Histology and Biomarker core, University of California San Francisco.

The publication costs of this article were defrayed in part by the payment of publication fees. Therefore, and solely to indicate this fact, this article is hereby marked "advertisement" in accordance with 18 USC section 1734.

Note

Supplementary data for this article are available at Clinical Cancer Research Online (http://clincancerres.aacrjournals.org/).

Received October 26, 2022; revised January 19, 2023; accepted March 10, 2023; published first March 14, 2023.

References

1. Siegel RL, Miller KD, Fuchs HE, Jemal A. Cancer statistics, 2022. CA Cancer J Clin 2022;72:7–33.
2. Parker C, Nilsson S, Heinrich D, Helle SI, O'Sullivan JM, Fosså SD, et al. Alpha emitter Radium-223 and survival in metastatic prostate cancer. N Engl J Med 2013;369:213–23.
3. Sartor O, de Bono J, Chi KN, Fizazi K, Herrmann K, Rahbar K, et al. Lutetium-177–PSMA-617 for metastatic castration-resistant prostate cancer. N Engl J Med 2021;385:1091–103.
4. Jones W, Griffiths K, Barata PC, Paller CJ. PSMA theranostics: review of the current status of PSMA-targeted imaging and radioligand therapy. Cancers 2020;12:1367.
5. Tosoian JJ, Gorin MA, Rowe SP, Andreas D, Szabo Z, Pienta KJ, et al. Correlation of PSMA-targeted 18F-DCFPyL PET/CT findings with immunohistochemical and genomic data in a patient with metastatic neuroendocrine prostate cancer. Clin Genitourin Cancer 2017;15:e65–8.
6. Usmani S, Ahmed N, Marafi F, Rasheed R, Amanguno HG, Al Kandari F. Molecular imaging in neuroendocrine differentiation of prostate cancer. Clin Nucl Med 2017;42:410–3.
7. Bakht MK, Derecichei I, Li Y, Ferraiuolo RM, Dunning M, Oh SW, et al. Neuroendocrine differentiation of prostate cancer leads to PSMA suppression. Endocr Relat Cancer 2019;26:131–46.
8. Wang B, Liu C, Wei Y, Meng J, Zhang Y, Gan H, et al. A prospective trial of 68Ga-PSMA and 18F-FDG PET/CT in nonmetastatic prostate cancer patients with an early PSA progression during castration. Clin Cancer Res 2020;26:4551–8.
9. Gafita A, Marcus C, Kostos L, Schuster DM, Calais J, Hofman MS. Predictors and real-world use of prostate-specific radioligand therapy: PSMA and beyond. Am Soc Clin Oncol Educ Book 2022;42:1–17.
10. Aggarwal R, Huang J, Alumkal JJ, Zhang L, Feng FY, Thomas Gv, et al. Clinical and genomic characterization of treatment-emergent small-cell neuroendocrine prostate cancer: a multi-institutional prospective study. J Clin Oncol 2018;36:2492.
11. Ruan W, Sassoon A, An F, Simko JP, Liu B. Identification of clinically significant tumor antigens by selecting phage antibody library on tumor cells *in situ* using laser capture microdissection. Mol Cell Proteomics 2006;5:2364–73.
12. Su Y, Bidlingmaier S, Lee NK, Liu B. Combine phage antibody display library selection on patient tissue specimens with laser capture microdissection to identify novel human antibodies targeting clinically relevant tumor antigens. Methods Mol Biol 2018;1701:331–47.
13. He J, Wang Y, Feng J, Zhu X, Lan X, Iyer AK, et al. Targeting prostate cancer cells in vivo using a rapidly internalizing novel human single-chain antibody fragment. J Nucl Med 2010;51:427–32.
14. Su Y, Liu Y, Behrens CR, Bidlingmaier S, Lee NK, Aggarwal R, et al. Targeting CD46 for both adenocarcinoma and neuroendocrine prostate cancer. JCI Insight 2018;3:e121497.
15. Russell S, Russell S. CD46: a complement regulator and pathogen receptor that mediates links between innate and acquired immune function. Tissue Antigens 2004;64:111–8.
16. Aggarwal RR, Vuky J, VanderWeele DJ, Rettig M, Heath EI, Beer TM, et al. Phase 1a/1b study of FOR46, an antibody drug conjugate (ADC), targeting CD46 in metastatic castration-resistant prostate cancer (mCRPC). J Clin Oncol 40: 16s, 2022 (suppl; abstr 3001).
17. Wang S, Li J, Hua J, Su Y, Beckford-Vera DR, Zhao W, et al. Molecular imaging of prostate cancer targeting CD46 using immunoPET. Clin Cancer Res 2021;27:1305–15.
18. Tafreshi NK, Doligalski ML, Tichacek CJ, Pandya DN, Budzevich MM, El-Haddad G, et al. Development of targeted alpha particle therapy for solid tumors. Molecules 2019;24:4314.
19. Langbein T, Chaussé G, Baum RP. Salivary gland toxicity of PSMA radioligand therapy: relevance and preventive strategies. J Nucl Med 2018;59:1172–3.
20. McDevitt MR, Thorek DLJ, Hashimoto T, Gondo T, Veach DR, Sharma SK, et al. Feed-forward alpha particle radiotherapy ablates androgen receptor-addicted prostate cancer. Nat Commun 2018;9:1629.
21. Miederer M, McDevitt MR, Sgouros G, Kramer K, Cheung N-Kv, Scheinberg DA. Pharmacokinetics, dosimetry, and toxicity of the targetable atomic generator, 225Ac-HuM195, in nonhuman primates. J Nucl Med 2004;45:129–37.
22. Bakht MK, Hayward JJ, Shahbazi-Raz F, Skubal M, Tamura R, Stringer KF, et al. Identification of alternative protein targets of glutamate-ureido-lysine associated with PSMA tracer uptake in prostate cancer cells. Proc Natl Acad Sci U S A 2022;119:e2025710119.
23. Hao J, Ci X, Xue H, Wu R, Dong X, Choi SYC, et al. Patient-derived hormone-naive prostate cancer xenograft models reveal growth factor receptor bound protein 10 as an androgen receptor-repressed gene driving the development of castration-resistant prostate cancer. Eur Urol 2018;73:949–60.
24. Akamatsu S, Wyatt AW, Lin D, Lysakowski S, Zhang F, Kim S, et al. The placental gene PEG10 promotes progression of neuroendocrine prostate cancer. Cell Rep 2015;12:922–36.
25. Maguire WF, McDevitt MR, Smith-Jones PM, Scheinberg DA. Efficient 1-step radiolabeling of monoclonal antibodies to high specific activity with 225Ac for α-particle radioimmunotherapy of cancer. J Nucl Med 2014;55:1492–8.
26. Sharma SK, Lyashchenko SK, Park HA, Pillarsetty N, Roux Y, Wu J, et al. A rapid bead-based radioligand binding assay for the determination of target-binding fraction and quality control of radiopharmaceuticals. Nucl Med Biol 2019;71:32–8.
27. Schwartz J, Jaggi JS, O'Donoghue JA, Ruan S, McDevitt M, Larson SM, et al. Renal uptake of bismuth-213 and its contribution to kidney radiation dose following administration of actinium-225-labeled antibody. Phys Med Biol 2011;56:721–33.
28. Jaggi JS, Kappel BJ, McDevitt MR, Sgouros G, Flombaum CD, Cabassa C, et al. Efforts to control the errant products of a targeted in vivo generator. Cancer Res 2005;65:4888–95.
29. Envigo. Radiosensitivity of immunodeficient mice in oncology studies. Available from: https://insights.envigo.com/hubfs/resources/white-papers/r2g2-mouse-comparative-model-radiosensitivity-white-paper.pdf.
30. Kratochwil C, Bruchertseifer F, Rathke H, Hohenfellner M, Giesel FL, Haberkorn U, et al. Targeted a-therapy of metastatic castration-resistant prostate cancer with 225 Ac-PSMA-617: swimmer-plot analysis suggests efficacy regarding duration of tumor control. J Nucl Med 2018;59:795–802.
31. Bronsert P, Reichel K, Ruf J. Loss of PSMA expression in non-neuroendocrine dedifferentiated acinar prostate cancer. Clin Nucl Med 2018;43:526–8.
32. Banerjee SR, Lisok A, Minn I, Josefsson A, Kumar V, Brummet M, et al. Preclinical evaluation of 213Bi- and 225Ac-labeled low-molecular-weight compounds for radiopharmaceutical therapy of prostate cancer. J Nucl Med 2021;62:980–8.
33. Bäck TA, Jennbacken K, Hagberg Thulin M, Lindegren S, Jensen H, Olafsen T, et al. Targeted alpha therapy with astatine-211-labeled anti-PSCA A11 minibody

shows antitumor efficacy in prostate cancer xenografts and bone microtumors. EJNMMI Res 2020;10:10.
34. Korsen JA, Gutierrez JA, Tully KM, Carter LM, Samuels Zv Khitrov S, et al. Delta-like ligand 3–targeted radioimmunotherapy for neuroendocrine prostate cancer. Proc Natl Acad Sci U S A 2022;119:e2203820119.
35. Zhao N, Chopra S, Trepka K, Wang Y-H, Sakhamuri S, Hooshdaran N, et al. CUB domain-containing protein 1 (CDCP1) is a target for radioligand therapy in castration-resistant prostate cancer, including PSMA null disease. Clin Cancer Res 2022;28:3066–75.
36. Essler M, Gärtner FC, Neff F, Blechert B, Senekowitsch-Schmidtke R, Bruchertseifer F, et al. Therapeutic efficacy and toxicity of 225Ac-labelled vs. 213Bi-labelled tumour-homing peptides in a preclinical mouse model of peritoneal carcinomatosis. Eur J Nucl Med Mol Imaging 2012;39:602–12.
37. de Kruijff RM, Raavé R, Kip A, Molkenboer-Kuenen J, Morgenstern A, Bruchertseifer F, et al. The *in vivo* fate of 225Ac daughter nuclides using polymersomes as a model carrier. Sci Rep 2019;9:11671.
38. Kozempel J, Mokhodoeva O, Vlk M. Progress in targeted alpha-particle therapy. What we learned about recoils release from *in vivo* generators. Molecules 2018; 23:581.
39. Lee W, Bobba KN, Kim JY, Park H, Bhise A, Kim W, et al. A short PEG linker alters the *in vivo* pharmacokinetics of trastuzumab to yield high-contrast immuno-PET images. J Mater Chem B 2021;9:2993–7.
40. Poty S, Carter LM, Mandleywala K, Membreno R, Abdel-Atti D, Ragupathi A, et al. Leveraging bioorthogonal click chemistry to improve 225 AC-radioimmunotherapy of pancreatic ductal adenocarcinoma. Clin Cancer Res 2019;25:868–80.
41. Burak ES, Mahoney SJ, Simms RW, Valliant JF, Burak ES, Mahoney SJ, et al. Fusion Pharmaceuticals Inc. Pharmacokinetic enhancements of bifunctional chelates and uses thereof; United States Patent, US 2019 /0030194 A1Jan 31(2019).
42. Li J, Huang T, Hua J, Wang Q, Su Y, Chen P, et al. CD46 targeted 212Pb alpha particle radioimmunotherapy for prostate cancer treatment. biorxiv 2022; 2022.10.14.512321. Available from: http://biorxiv.org/content/early/2022/10/18/2022.10.14.512321.abstract.